

Magnetic Skyrmions in a Hall Balance with Interfacial Canted Magnetizations

Jingyan Zhang, Ying Zhang, Yang Gao, Guoping Zhao,* Lei Qiu, Kaiyou Wang, Pengwei Dou, Wenlin Peng, Yuan Zhuang, Yanfei Wu, Guoqiang Yu, Zhaozhao Zhu, Yunchi Zhao, Yaqin Guo, Tao Zhu, Jianwang Cai, Baogen Shen, and Shouguo Wang*

Magnetic skyrmions are attracting interest as efficient information-storage devices with low energy consumption, and have been experimentally and theoretically investigated in multilayers including ferromagnets, ferrimagnets, and antiferromagnets. The 3D spin texture of skyrmions demonstrated in ferromagnetic multilayers provides a powerful pathway for understanding the stabilization of ferromagnetic skyrmions. However, the manipulation mechanism of skyrmions in antiferromagnets is still lacking. A Hall balance with a ferromagnet/insulating spacer/ferromagnet structure is considered to be a promising candidate to study skyrmions in synthetic antiferromagnets. Here, high-density Néel-type skyrmions are experimentally observed at zero field and room temperature by Lorentz transmission electron microscopy in a Hall balance (core structure $[\text{Co}/\text{Pt}]_n/\text{NiO}/[\text{Co}/\text{Pt}]_n$) with interfacial canted magnetizations because of interlayer ferromagnetic/antiferromagnetic coupling between top and bottom $[\text{Co}/\text{Pt}]_n$ multilayers, where the Co layers in $[\text{Co}/\text{Pt}]_n$ are always ferromagnetically coupled. Micromagnetic simulations show that the generation and density of skyrmions are strongly dependent on interlayer exchange coupling (IEC) and easy-axis orientation. Direct experimental evidence of skyrmions in synthetic antiferromagnets is provided, suggesting that the proposed approach offers a promising alternative mechanism for room-temperature spintronics.

energetically favorable because of the competition among various magnetic interactions,^[10–13] where the skyrmions can be stabilized by tuning the stack sequences and external excitations.^[14–17] For example, the local injection of a spin-polarized current can be used to promote skyrmion nucleation.^[18] Extensive research into skyrmions and their dynamics near room temperature (RT) in ferromagnets has greatly extended their use in spintronic devices because of their robust thermal stability and tunability.^[19–25] However, the skyrmion Hall effect (SkHE), observed as a deflection with respect to the current direction, leads to the lateral accumulation and annihilation of skyrmions,^[26] which greatly hinders ferromagnetic skyrmion-based applications. These fundamental limitations are being addressed by investigating the behavior of skyrmions in ferrimagnets and antiferromagnets.

The skyrmions in ferrimagnets can be detected because of partially compensated magnetization, consistent with previous theoretical predictions.^[27,28] Antiferromagnets could overcome the limitations of ferromagnetic skyrmions by taking advantage of their fast domain wall motion and absence of stray fields.^[29,30] Furthermore, it has been theoretically demonstrated that the SkHE finally vanishes in antiferromagnets because of the symmetry of the two opposite spin

Magnetic skyrmions, with a topologically protected nontrivial spin texture, have been widely investigated for potential applications in devices with ultralow power consumption, such as logic, memory, and neuromorphic computing bits.^[1–9] The generation of this exotic spin texture in the multilayers is

magnets could overcome the limitations of ferromagnetic skyrmions by taking advantage of their fast domain wall motion and absence of stray fields.^[29,30] Furthermore, it has been theoretically demonstrated that the SkHE finally vanishes in antiferromagnets because of the symmetry of the two opposite spin

Dr. J. Zhang, P. Dou, W. Peng, Y. Zhuang, Dr. Y. Wu, Prof. S. Wang
School of Materials Science and Engineering
Beijing Advanced Innovation Center for Materials Genome Engineering
University of Science and Technology Beijing
Beijing 100083, China
E-mail: sgwang@ustb.edu.cn

Prof. Y. Zhang, Y. Gao, Prof. G. Yu, Z. Zhu, Dr. Y. Zhao, Y. Guo,
Prof. T. Zhu, Prof. J. Cai, Prof. B. Shen
State Key Laboratory of Magnetism
Beijing National Laboratory for Condensed Matter Physics
Institute of Physics
Chinese Academy of Sciences
Beijing 100190, China

 The ORCID identification number(s) for the author(s) of this article can be found under <https://doi.org/10.1002/adma.201907452>.

Prof. G. Zhao, L. Qiu
College of Physics and Electronic Engineering
Sichuan Normal University
Chengdu 610068, China
E-mail: zhaogp@uestc.edu.cn

Prof. K. Wang
State Key Laboratory for Superlattices and Microstructures
Institute of Semiconductors
Chinese Academy of Sciences
Beijing 100083, China

DOI: 10.1002/adma.201907452

lattices.^[31,32] Unfortunately, completely compensated magnetizations in ideal antiferromagnets result in challenges related to the detection and manipulation of antiferromagnetic skyrmions.^[33–35] Fortunately, chiral behavior including interlayer Dzyaloshinskii–Moriya interactions (DMI) and stabilized skyrmions has been demonstrated in synthetic antiferromagnets (SAFs),^[36–39] where the alignment of the magnetic moments can be tuned by manipulating two ferromagnetic layers coupled antiferromagnetically.^[40,41] However, the microscopic origin of skyrmion generation is complicated, where opposite skyrmions in SAFs with two ferromagnetic layers have been theoretically proposed.^[42,43] Recently, the 3D spin texture of skyrmions associated with their depth-dependent evolution was observed in ferromagnetic multilayers.^[23,44,45] Therefore, it is essential to perform detailed structural analyzes and experimental manipulation of skyrmions in SAFs, which will greatly enhance the understanding of the physical mechanism and assist further design of 3D skyrmions-based devices. A Hall balance with a $[\text{Co}/\text{Pt}]_4/\text{NiO}/[\text{Co}/\text{Pt}]_4$ structure was used here to investigate the chiral spin textures. A Hall balance has been proposed experimentally^[40,41] to realize multi-state storage, where the interlayer coupling between top and bottom $[\text{Co}/\text{Pt}]_n$ multilayers is highly sensitive to the NiO spacer thickness. In a Hall balance, the interlayer exchange coupling (IEC) between the antiferromagnetic and ferromagnetic couplings can be successfully tuned by varying NiO thickness. Furthermore, the insulating NiO spacer could provide a promising approach for tuning the spin structure by electric-control (current/voltage). We report the experimental observation of high-density Néel-type skyrmions at RT using Lorentz- transmission electron microscopy (L-TEM) in a Hall balance with canted magnetizations. The micromagnetic simulation further proves that the tilting of the easy axis can reduce the degree of difficulty (IEC strength) to generate skyrmions, which is in good agreement with the canted magnetizations identified by polarized neutron reflectometry. Our findings are expected to provide greater freedom to effectively manipulate the chiral behavior in such systems.

Two configurations, with parallel/antiparallel alignments of the magnetic moments, have been confirmed in SAFs with two ferromagnetic layers separated by an ultrathin spacer (metal or oxide layer). In our previous studies, using the novel concept of SAFs with a core structure of $[\text{Co}/\text{Pt}]_n/\text{NiO}/[\text{Co}/\text{Pt}]_n$ based on out-of-plane ferromagnetic layers, namely a Hall balance, we achieved multistate storage and logic in a single cell.^[40,41] In this study, we use the Hall balance to investigate the topological properties of such structures. The core structure of the sputtered Hall balance is shown schematically in **Figure 1a**, where the interfacial DMI is very small because of the symmetry of the multilayers. A vertical pure spin current generated from the Pt layer due to spin Hall effect can be injected into ferromagnetic layers to generate a spin-orbit torque when an in-plane current flows in a bottom Pt layer. It was demonstrated that the spin-orbit torque could induce the magnetization switching of the adjacent magnetic layer.^[9] The bottom Pt layer serves as a spin-current source to generate spin-orbit torque, which facilitates the generation of magnetic skyrmions. In general, the strength and type of IEC, including ferromagnetic coupling (FMC) and antiferromagnetic coupling (AFMC), are highly sensitive to the properties of the

multilayered structure, such as the Co/Pt atomic ratio, period number, and NiO-layer thickness (t_{NiO}). We therefore fabricated a series of multilayers with different NiO thicknesses to control IEC; the interfacial DMI and total magnetization are not highly dependent on t_{NiO} . For the sputtered Hall balance multilayers, a very sharp interface between the $[\text{Co}/\text{Pt}]_4$ multilayers and NiO spacer was clearly observed (Figure S1, Supporting Information). Further details regarding the structural characterization of the samples are provided in the supporting information. We used the shift of the minor loop (H_{ex}) to quantify the IEC strength, and observed a strong dependence on t_{NiO} . Figure 1b shows H_{ex} as a function of t_{NiO} , where the oscillation of the H_{ex} curve indicates the large tunability of IEC by varying t_{NiO} . In addition, an IEC oscillation between the FMC and AFMC was observed, with a period of $t_{\text{NiO}} = 0.4$ nm. We attribute this to the modulation of multiple electron-wave reflections induced by the antiferromagnetic order in the (111) NiO plane.^[46] The different IEC behavior leads to different spin configurations, which can be detected in the magnetic hysteresis (M – H) loops of typical samples in external fields applied perpendicularly to the film, as shown in Figure 1c. The M – H loop for $t_{\text{NiO}} = 1.3$ nm indicates that the antiferromagnetic state occurred in the positive field (nearly zero field), when the field was decreased from positive to negative saturation. Therefore, it is reasonable to conclude that the M – H loop for $t_{\text{NiO}} = 1.3$ nm results from IEC. Perpendicular magnetic anisotropy was observed in the Hall balance for various t_{NiO} values for both the AFMC and FMC states in the multilayered structure. Multiswitching in the M – H loop (red circle in Figure 1c) was clearly observed for the sample ($t_{\text{NiO}} = 1.3$ nm) with $H_{\text{ex}} \approx 203$ Oe (Figure S2, Supporting Information), indicating the existence of AFMC between the top and bottom $[\text{Co}/\text{Pt}]_4$ multilayers. Furthermore, the remnant magnetization (at zero field) was not zero in Figure 1c, suggesting that the magnetizations of the two $[\text{Co}/\text{Pt}]_n$ multilayers were opposite, but not strictly equal. The spin configuration will be characterized by the polarized neutron reflectometry. In contrast, only two stable states were obtained in the synthetic FMC structure (blue square in Figure 1c), where direct magnetic coupling occurred between the top and bottom $[\text{Co}/\text{Pt}]_4$ multilayers with $t_{\text{NiO}} = 1.0$ nm. The Hall loops for the sample with $t_{\text{NiO}} = 1.0$ and 1.3 nm are shown in Figure S2c,d (Supporting Information). The saturation ρ_{xy} was 0.97 and 0.95 $\mu\Omega$ cm for $t_{\text{NiO}} = 1.0$ nm and $t_{\text{NiO}} = 1.3$ nm, respectively, nearly independent on t_{NiO} as observed previously.^[41] However, the resistance state of the sample is highly sensitive to t_{NiO} , thus providing a simple way to tune its state. For example, only two configurations were observed in the FMC sample with $t_{\text{NiO}} = 1.0$ nm (Figure S2c, Supporting Information), whereas an additional resistance state was observed in the AFMC Hall balance with $t_{\text{NiO}} = 1.3$ nm (Figure S2d, Supporting Information). The high ρ_{xy} value for the sample with $t_{\text{NiO}} = 1.3$ nm was achieved for the parallel state of the two $[\text{Co}/\text{Pt}]_4$ multilayers (e.g., in a magnetic field of 650 Oe). When the field is decreased from 650 to 0 Oe, the magnetic configuration of the two $[\text{Co}/\text{Pt}]_4$ multilayers becomes antiparallel, resulting in a low ρ_{xy} value. The positive slope of Hall effect at high fields (inset of Figure S2c, Supporting Information) indicates hole-like transport in these multilayers.

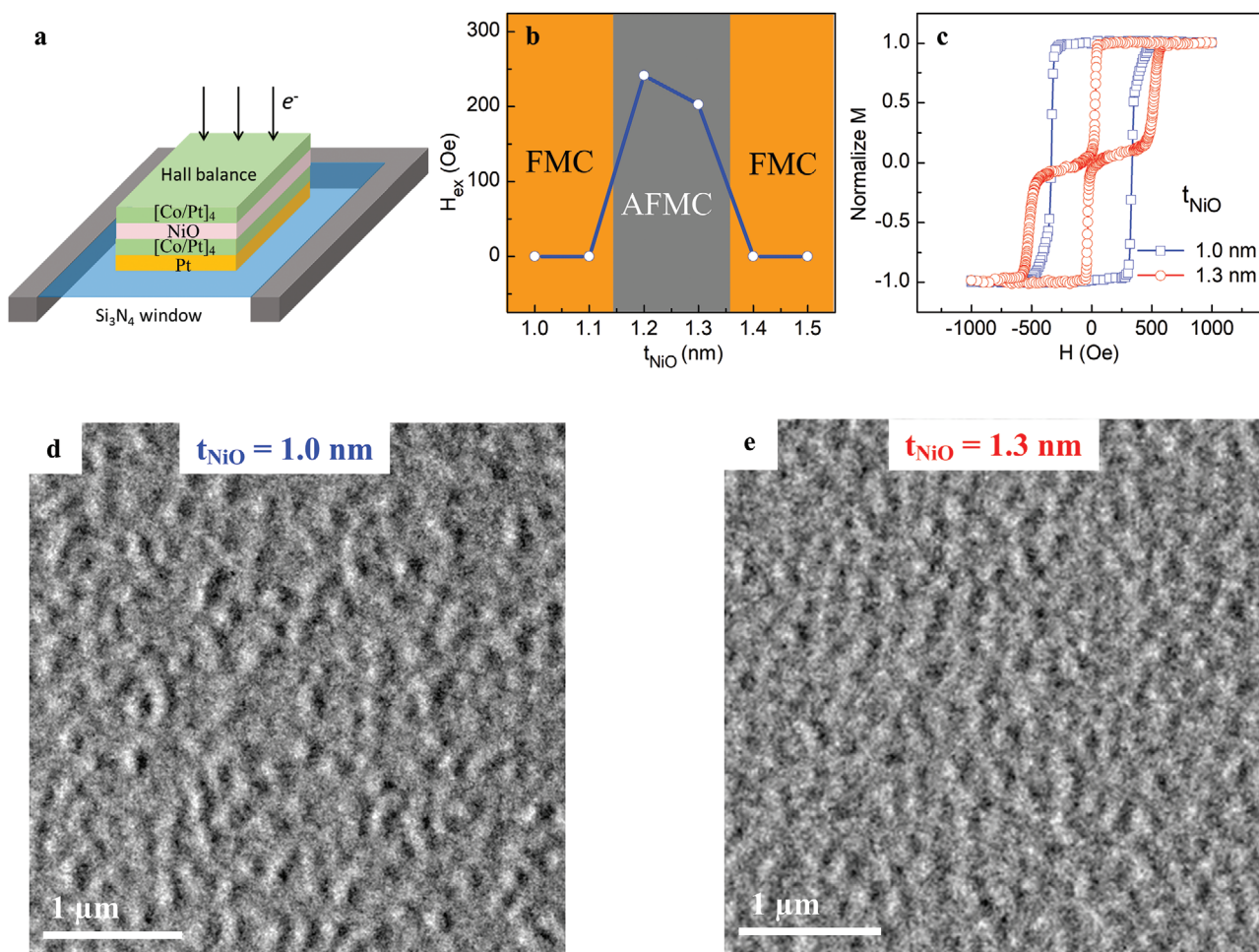


Figure 1. a) Schematic illustration of experimental geometry for L-TEM imaging, where the dimensions of Si_3N_4 membrane were $0.1 \text{ mm} \times 0.1 \text{ mm} \times 10 \text{ nm}$. A typical Hall balance with a core structure of $[\text{Co}/\text{Pt}]_n/\text{NiO}/[\text{Co}/\text{Pt}]_n$ was used. b) Shifted field H_{ex} of the minor loop as a function of t_{NiO} . c) Normalized $M-H$ loops for the samples with $t_{\text{NiO}} = 1.0 \text{ nm}$ (blue squares) and 1.3 nm (red circles) with external fields applied perpendicular to the films. L-TEM images of $[\text{Co}/\text{Pt}]_n/\text{NiO}/[\text{Co}/\text{Pt}]_n$ multilayers with FMC and AFMC were collected at zero fields with an angle of $+15^\circ$. d,e) High density of skyrmions in the Hall balance with different IEC (i.e., various t_{NiO} values).

To characterize the magnetic domains directly by L-TEM, the Hall balance with various t_{NiO} was deposited directly onto a Si_3N_4 membrane using the same growth parameters. The L-TEM images show almost no magnetic contrast for the Hall balance with AFMC and FMC (Figure S3, Supporting Information). We applied simultaneous external excitation with a pulsed electric current and a perpendicular magnetic field to individual samples with FMC and AFMC at RT and then completely removed the external excitations. High-density skyrmions at zero fields were clearly observed in the L-TEM images in multilayers with both $t_{\text{NiO}} = 1.0$ and 1.3 nm (Figure 1d,e, respectively), where the skyrmions density was $\approx 7.5 \mu\text{m}^{-2}$. The manipulation procedure using external fields in combination with in-plane electric currents and perpendicular magnetic fields to generate skyrmions is similar to that in a previous study on conventional ferromagnetic multilayers.^[16] However, the mechanism and magnetization dynamics in the Hall balance with FMC/AFMC need to be explored further. Experimental observation of high-density skyrmions in a Hall balance with varied IEC provides a novel

approach to investigate the topological behavior in synthetic antiferromagnets.

Domain structures can be analyzed by tilting the L-TEM specimens to change the contrast. Néel-type skyrmions have been confirmed experimentally using this method, where an obvious contrast reversal at relatively opposite angles and the disappearance of contrast at nearly 0° were observed.^[14,22] We performed L-TEM at zero fields for tilt angles of -15° , 0° , and $+15^\circ$, as shown in Figure 2a–c, respectively. We observed bright and dark regions with good contrast for the selected skyrmions at a tilting angle of -15° . For the opposite angle of $+15^\circ$, the reversed bright and dark magnetic contrast was clearly observed, while no magnetic contrast was observed at 0° . This contrast behavior was attributed to the existence of Néel-type skyrmions in our Hall balance with both FMC and AFMC, whose configuration is shown in Figure 2e. Generally, the energy of a skyrmion ($4\sqrt{AK} - \pi|D|$) is always smaller than that of a conventional domain wall ($4\sqrt{AK}$), and thus the Néel-type spin texture is preferred.^[47,48] The right insets of Figure 2d show enlarged images of the selected single skyrmion for tilt angles

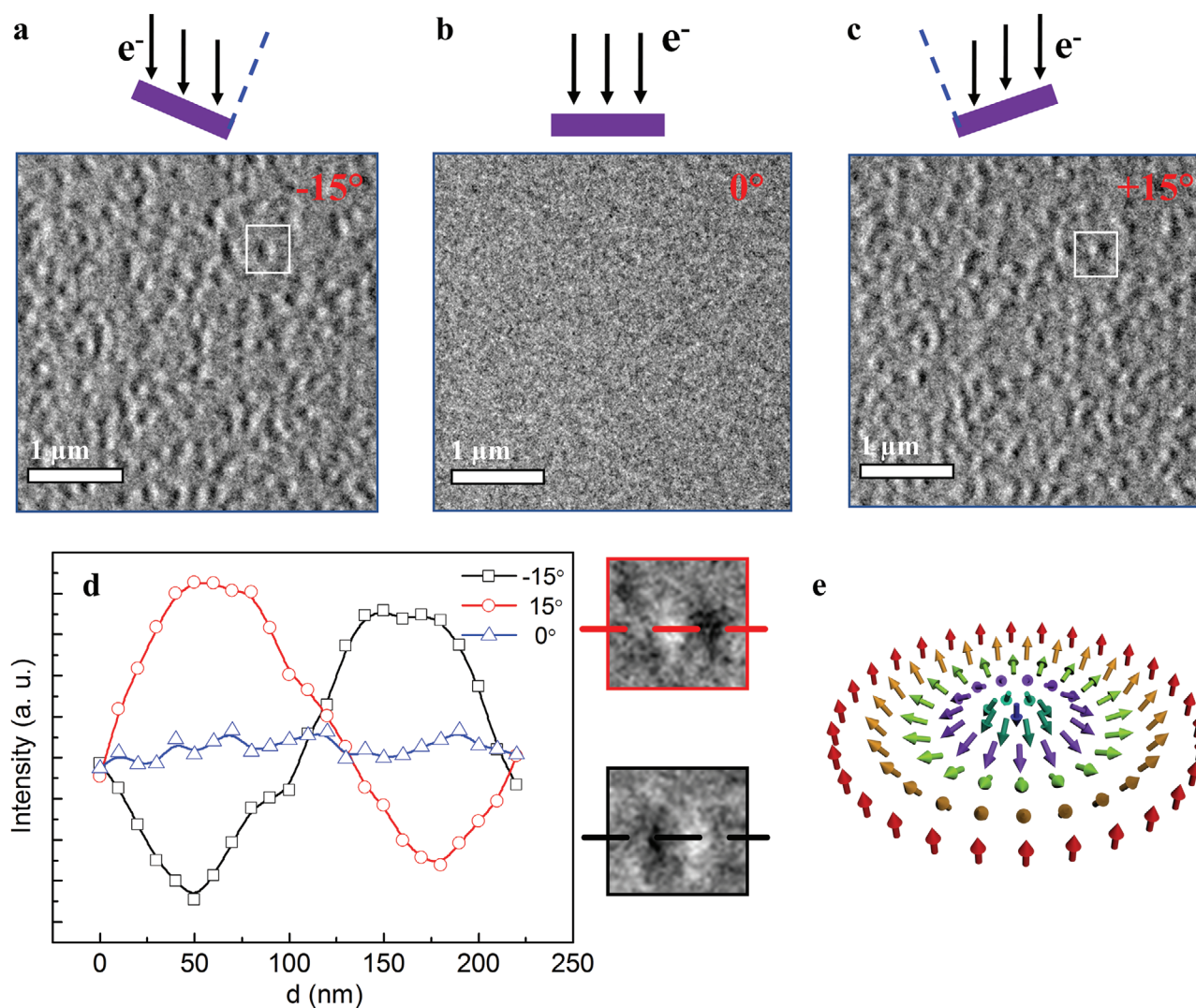


Figure 2. L-TEM images of the Néel-type skyrmion at zero fields for various tilting angles. a–c) Magnetic skyrmion images for a sample with $t_{\text{NiO}} = 1.3$ nm and AFMC, at tilting angles of -15° (a), 0° (b), and $+15^\circ$ (c), showing the disappearance of contrast at 0° and contrast reversal for opposite angles. d) Line profiles of three images along the transverse axis of the skyrmions showing the contrast differences. Enlarged skyrmions with a radius of 90 nm are indicated. e) Schematic of the spin structures for Néel-type skyrmions in our experiments.

of $\pm 15^\circ$. The intensity asymmetry of these magnetic skyrmions indicates polarities of +1 and -1, respectively, from the asymmetry direction (bright–dark or dark–bright). We obtained line profiles of the images at various tilt angles along the transverse axis of the skyrmions, while the intensity contrasts of the three images at various tilt angles are shown in Figure 2d. The size of a magnetic skyrmion was determined by the distance between the maximum and minimum value of a certain tilt angle, which provided a radius of about 90 nm for our samples. During the current-induced skyrmion creation process, the type and size of skyrmions for AFMC and FMC samples is not be changed by external magnetic fields, although the density varies (Figure S4, Supporting Information).

Polarized neutron reflectometry (PNR) is a powerful tool for analyzing the magnetic structures in thin films, as it is highly sensitive to in-plane magnetization but insensitive to perpendicular magnetization in magnetic films or multilayers.^[49,50] We

used PNR to quantitatively analyze the magnetic moments and their orientations. The magnetic scattering of the neutrons with spin-up and spin-down leads to different momentum-transfer (Q) dependences of the reflectivity curves (R^{++} and R^{--} , respectively). The ratio R^{++}/R^{--} is the non-spin-flip reflectivity, for which the neutron spin is parallel and antiparallel to the magnetic field, respectively. The spin asymmetry (SA) is defined as $(R^{++} - R^{--})/(R^{++} + R^{--})$, which is very sensitive to the in-plane magnetization of the film (components with $M//Q$). **Figure 3a,b** shows the R^{++} (red square) and R^{--} (blue circle) as functions of Q measured under in-plane magnetic fields of 20 Oe and 9000 Oe, respectively, for a Hall balance with AFMC ($t_{\text{NiO}} = 1.3$ nm). The depth dependence of the neutron and magnetic scattering-length density (SLD) profiles were extracted by fitting the reflectivity data using GenX software.^[51] When the applied magnetic field (such as 9000 Oe) is larger than the saturation field, all magnetic moments are forced to lie in-plane, leading

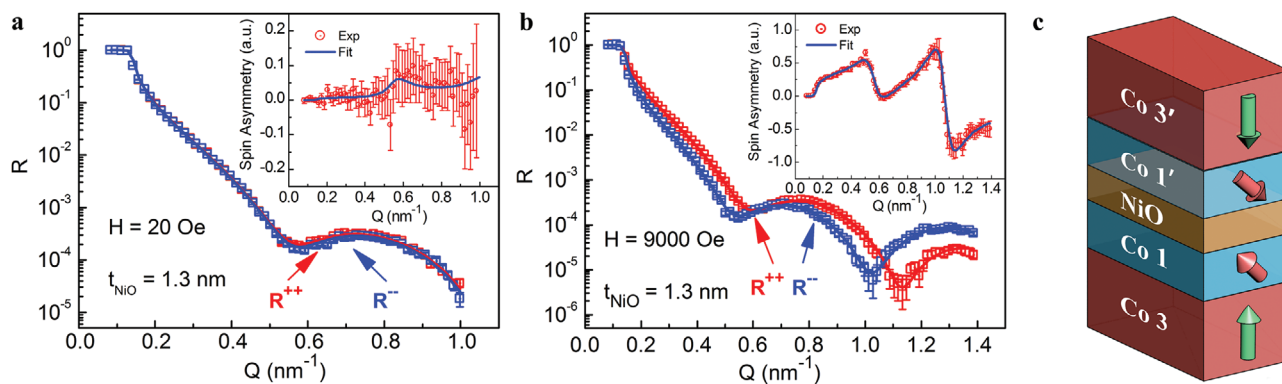


Figure 3. a,b) PNR spectra showing R^{++} (red squares) and R^{-} (blue circles) as a function of Q measured with in-plane magnetic fields of 20 Oe (a) and 9000 Oe (b) for the Hall balance with AFMC ($t_{\text{NiO}} = 1.3$ nm). The insets show the related spin asymmetry. c) Schematic of the magnetic structure of the multilayers with AFMC at RT.

to significant differences between the R^{++} and R^{-} reflectivity curves. However, when a very low magnetic field (such as 20 Oe) is applied, the R^{++} and R^{-} reflectivity curves overlap almost completely, as shown in Figure 3a. This is because magnetic neutron scattering is only sensitive to the components with $M//Q$. In contrast, the weak nonzero SA exhibits a small in-plane magnetization component, as shown in the inset of Figure 3a, strongly indicating the existence of canted magnetizations in the sample. We schematically illustrate the spin structure of a Hall balance with AFMC in Figure 3c. Note that whenever IEC is AFMC, canted magnetizations adjacent to the NiO spacer were clearly observed, although these had ideally been thought to be perpendicular. The angle of the canted magnetic moments was nearly 7° for multilayers with $t_{\text{NiO}} = 1.3$ nm. A similar behavior was observed for the FMC multilayers with $t_{\text{NiO}} = 1.0$ nm, as shown in Figure S5 (Supporting Information), with an angle of 4° . These PNR results are a confirmation of the existence for canted magnetic structure in synthetic antiferromagnets, which significantly enhances our understanding of the physical mechanism of topological spin textures, such as magnetic skyrmions.

The micromagnetic simulation has been considered as a quick and powerful tool,^[34,42,52,53] which is used to study magnetic skyrmions in our Hall balance. Figure 4 shows the skyrmion density (η_k) as a function of IEC energy (E_{IEC}) and the angle θ of the easy axis (EA). For perpendicular magnetic anisotropy with $\theta = 90^\circ$, the ideal η_k for typical values of E_{IEC} is shown in Figure 4a. No skyrmions can be stabilized when $E_{\text{IEC}} < -1.4$ mJ m $^{-2}$. For $E_{\text{IEC}} = -1.5$ mJ m $^{-2}$, a maximum value of $\eta_k \approx 100$ μm^{-2} was observed. Further increasing E_{IEC} resulted in a significant decrease in η_k , indicating that the E_{IEC} plays a decisive role in skyrmion nucleation. For a systematic comparison, we present a contour map of η_k as a function of E_{IEC} and θ in Figure 4b, where the blue region represents the area with no skyrmions. The white line indicates the critical boundary of E_{IEC} , beyond which skyrmions can be generated. For example, the critical value of E_{IEC} is -1.31 mJ m $^{-2}$ for $\theta = 85^\circ$ and increases to -1.45 mJ m $^{-2}$ for $\theta = 90^\circ$, indicating that the easy axis affects the E_{IEC} region of the maximum η_k . However, for even larger negative E_{IEC} values, where skyrmions can be nucleated, η_k remains considerably lower (≈ 25 μm^{-2} , as marked by the green area) than that of the red region (≈ 100 μm^{-2}). In

order to tune η_k , an external excitation (in-plane current and perpendicular magnetic field) is applied. Figure 4c shows the skyrmion number (density) for typical E_{IEC} values under simultaneous excitation. The positive and negative E_{IEC} values correspond to FMC and AFMC, respectively. The domains and skyrmions remain stabilized when the applied external excitations are removed. There was a significant change in the skyrmion number (density) obtained over a wide energy region. Although E_{IEC} is extremely low (0.1 mJ m $^{-2}$), a high density of Néel-type skyrmions was observed, suggesting that the energy region for skyrmion nucleation was much wider than that of multilayers without external excitations. The skyrmion number (density) as a function of E_{IEC} is plotted in Figure 4d. Note that the skyrmion density in multilayers with both FMC (positive energy) and AFMC (negative energy) was high, which is in good agreement with our experimental results. A detailed discussion of skyrmion generation, where the skyrmions in the Hall balance with ground state and external excitation were simulated, is provided in the supporting information. In the ground state, the antiparallel magnetization alignments (including the opposite skyrmions) formed in the Hall balance with various E_{IEC} (Figures S6 and S7, Supporting Information). After the external excitation was removed, the current injected into the bottom Pt layer play an effect on both top and bottom [Co/Pt] multilayers in a Hall balance with weak E_{IEC} , leading to different variations in the domain structure. The skyrmions will form in both the top and bottom ferromagnetic layer for the Hall balance with various IECs, as shown in Figure S7 (Supporting Information). These simulations provide a novel perspective for understanding the high density skyrmion induced by external excitation in the Hall balance with AFMC and FMC. We conclude that magnetic skyrmions can be generated over a wide range of E_{IEC} , although η_k in our experiments was slightly lower than the predicted value, which may be because of a smaller DMI in the Hall balance compared to the theoretical values. Our simulations, together with the experimental results, demonstrate an efficient method for controlling the nucleation and density of skyrmions, which is a critical for manipulating the skyrmion storage density, by tuning the IEC and the EA angle. In addition to the nucleation of skyrmion in the Hall balance, the dynamics under a pulse current should be paid more attention. The effort has been taken to drive skyrmion motion by

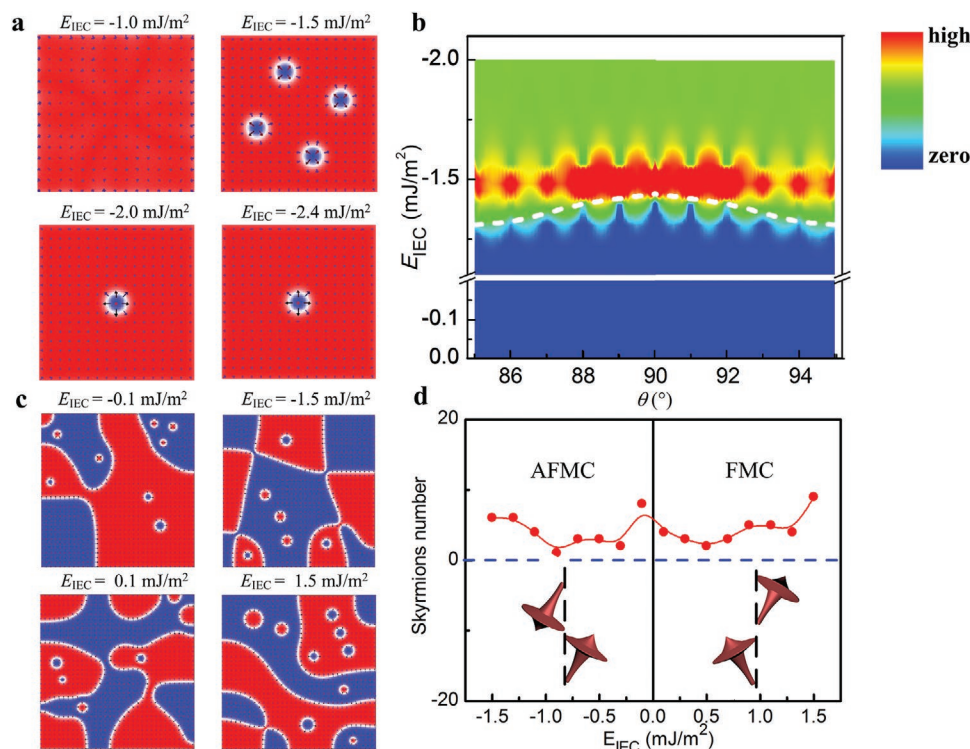


Figure 4. Micromagnetic simulation of skyrmions for various E_{IEC} and the angle (θ) values of EA. a) The simulated volume has an area of $200 \text{ nm} \times 200 \text{ nm}$ and a thickness of 9 nm . The spin configuration for the bottom layer is shown. The EA is normal to the film with $\theta = 90^\circ$, and the stable magnetization distribution is shown for $E_{\text{IEC}} = -1.0, -1.5, -2.0,$ and -2.4 mJ m^{-2} . b) Contour map of the extracted skyrmion density as a function of E_{IEC} and θ without external excitation. The critical boundary of IEC energy for the emergence of skyrmions is shown by the white dashed line, where the high value is $100 \mu\text{m}^{-2}$ in our micromagnetic model. c) Stable magnetization distribution for various IEC energies, including FMC (positive energy) and AFMC (negative energy), where the excitation (in-plane current and perpendicular magnetic field) is removed. The simulated volume has an area of $400 \text{ nm} \times 400 \text{ nm}$ and a thickness of 9 nm . The spin configuration for the top layer is shown. d) The skyrmion number as a function of IEC energy. The two insets represent the spin configuration in the Hall balance with FM and AFM coupling.

various pulse currents. Unfortunately, no movement has yet been clearly observed, which may be due to the strong pinning effect and low current density in our Hall balance. Meanwhile, some technological difficulties (such as micro/nanofabrication of the sample deposited on thin Si_3N_4 membranes) should be solved in further studies on skyrmion motion. Our simulations indicate that the skyrmion Hall angle can be significantly suppressed, as shown in Figure S9 and Video S1 (Supporting Information), while the skyrmion in the Hall balance with AFMC was driven by a pulse current. Recently, it has been demonstrated that the pinning effect plays an effective role in skyrmion dynamics.^[54,55] Furthermore, a comparison between the skyrmion motion of antiferromagnets and ferromagnets in the presence of a defect was presented, where the defect has a more important role in antiferromagnets compared with ferromagnets.^[56] It is reasonable to expect that the motion of the skyrmions in a Hall balance with AFMC should be effectively slowed down or even captured when defects exist in the channel.

In conclusion, high-density Néel-type skyrmions were observed at RT using L-TEM of the Hall balance with FM and AFM couplings, where the magnetic moments were confirmed by PNR to be canted in both the bottom and the top $[\text{Co}/\text{Pt}]_n$ multilayers. Our micromagnetic simulations provide new insights into the underlying physics about the formation and

density of skyrmions, together with its dependence on E_{IEC} and the easy axis. Further work to investigate the dynamics and the electric control of skyrmions is in progress. Our findings highlight the possibility of engineering skyrmion-based spintronic devices in robust synthetic antiferromagnets in the near future.

Experimental Section

Sample Fabrication and Magnetic Characterization: The films/multilayers were deposited simultaneously on thermally oxidized Si wafers and Si_3N_4 membranes using magnetron sputtering (AJA, ATC-2200) at RT. The core stack was $\text{Pt}(3 \text{ nm})/[\text{Co}(0.4 \text{ nm})/\text{Pt}(0.8 \text{ nm})]_4/\text{NiO}/[\text{Co}(0.4 \text{ nm})/\text{Pt}(0.8 \text{ nm})]_4$, where the metal and oxide layers were prepared by direct current (DC) and radio frequency (RF) magnetron sputtering, respectively. The base pressure was $<6 \times 10^{-6} \text{ Pa}$, and a working pressure of Ar at 0.5 Pa during sputtering was maintained. The films deposited on thermally oxidized Si wafers were used for magnetic measurements with vibrating sample magnetometry (Model 4HF), where the external magnetic fields were applied in-plane or perpendicular to the films.

Real-Space Structural Images: Structural analysis was performed using high-resolution TEM (Tecnai F20). L-TEM (JEOL 2100F) was used for magnetic domain imaging of the films deposited onto Si_3N_4 membranes. To determine the spin structure of the skyrmions, three sets of images were obtained (at positive, negative, and zero angles) using a charge-coupled device camera. During imaging, the out-of-plane

magnetic fields were tuned by varying the strength of the microscope objective-lens current.

Polarized Neutron Reflectometry Measurements: The PNR measurements were conducted using the Multipurpose Reflectometer at the China Spallation Neutron Source. The neutron reflectivity curves were recorded at RT as a function of the momentum transfer $Q = 4\pi \sin \theta/\lambda$, where λ is the neutron wavelength and θ is the angle of incidence between the neutron beam and the film plane. To access a broad momentum-transfer range, the reflected neutrons were collected at different angles of incidence.

Spin-Dependent Transport Measurements: After film growth, the samples were patterned into a Hall cross with widths of 10 μm using standard lithography and ion milling methods. A Keithley 6221 current source and a 2182A nanovoltmeter were used for the DC Hall-voltage measurements at RT, where a current of 1 mA was applied to eliminate thermal effects.

Micromagnetic Simulations: The simulations were performed using the Object-Oriented Micromagnetic Framework (OOMMF) to investigate the dependence of skyrmions on E_{IEC} and the EA angle. The model included two coupled [Co/Pt]₄ layers separated by 1 nm, where each Co/Pt was 1 nm thick. The layers had an area of 400 nm \times 400 nm. The unit cell was 2 nm \times 2 nm \times 0.5 nm, which was sufficiently smaller than the typical exchange length and the skyrmion size, ensuring a balance between numerical accuracy and computational efficiency. The blue and red regions represented spin point-out and point-in vertical to the plane, respectively. The angle of the EA was the angle between easy axis and the film plane. The main external excitation parameters were: the current density $j = 1.9 \times 10^9 \text{ A m}^{-2}$, the magnetic field $H = 50 \text{ Oe}$, and duration of the current and magnetic field $t = 2 \text{ ns}$. The AFM and/or FM coupling strength was tuned during simulation, where the AFM and FM coupling strength was from -2.4 to -0.1 mJ m^{-2} and from 0.1 to 1.5 mJ m^{-2} , respectively. The spin dynamics was controlled by the Landau–Lifshitz–Gilbert (LLG) equation

$$\frac{dM}{dt} = \gamma H_{\text{eff}} \times M + \frac{\alpha}{M_s} M \times \frac{dM}{dt} \quad (1)$$

where the Gilbert gyromagnetic ratio $\gamma = 2.21 \times 10^5 \text{ m A}^{-1} \text{ s}^{-1}$, the damping constant $\alpha = 0.3$, and the saturation magnetization $M_s = 580 \text{ kA m}^{-1}$. Here, H_{eff} is the effective field, given by

$$H_{\text{eff}} = -\mu_0^{-1} \frac{\partial(E_T + E_B + E_{\text{inter}})}{\partial M} \quad (2)$$

An AFMC energy exists between the top and the bottom FM layers, which is expressed by

$$E_{\text{inter}} = \int ds A_{\text{inter}} \left[\left(\frac{M^T M^B}{M_s^2} \right) \right] \quad (3)$$

The average energy for each layer can be expressed by

$$E_{\text{intra}} = \int dv A_{\text{intra}} \left[\nabla \left(\frac{M^\tau}{M_s} \right) \right]^2 - K \frac{(n \cdot M^\tau)^2}{M_s^2} - \frac{\mu_0}{2} M^\tau H_d(M^\tau) + \frac{D}{M_s^2} \left(M_z^\tau \frac{\partial M_x^\tau}{\partial x} + M_z^\tau \frac{\partial M_y^\tau}{\partial y} - M_x^\tau \frac{\partial M_x^\tau}{\partial x} - M_y^\tau \frac{\partial M_y^\tau}{\partial y} \right) \quad (4)$$

where τ is the layer index ($\tau = T, B$), and the magnetic coupling energy A_{intra} within the top/bottom Co/Pt layer is 15 pJ m^{-1} . The anisotropy constant is $K = 0.8 \text{ MJ m}^{-3}$, and the EA angle is 85° – 95° . Here, $H_d(M)$ is the demagnetization field, and the DMI strength is 3 mJ m^{-2} , μ_0 is the vacuum permeability constant, and n is the unit surface-normal vector.

Supporting Information

Supporting Information is available from the Wiley Online Library or from the author.

Acknowledgements

J.Y.Z. and Ying Zhang contributed equally to this work. This work was supported by the National Key Research and Development Program of China (Grant No. 2019YFB2005800), the Natural Science Foundation of China (Grant Nos. 11874082, 11874408, 11874409, 51625101, 51431009, 51771127, and 51971026), the ISF-NSFC Joint Research Program (Grant Nos. 51961145305), the State Key Laboratory for Advanced Metals and Materials (Grant No. 2019Z-10), Beijing Natural Science Foundation Key Program (Grant Nos. Z190007 and Z190009), and the Fundamental Research Funds for the Central Universities Grant FRF-TP-16-001C2.

Conflict of Interest

The authors declare no conflict of interest.

Keywords

interfacial canted magnetizations, interlayer exchange coupling, skyrmions, synthetic antiferromagnets

Received: November 13, 2019

Revised: June 29, 2020

Published online:

- [1] A. Fert, N. Reyren, V. Cros, *Nat. Rev. Mater.* **2017**, *2*, 17031.
- [2] N. Nagaosa, Y. Tokura, *Nat. Nanotechnol.* **2013**, *8*, 899.
- [3] K. Karube, J. S. White, N. Reynolds, J. L. Gavilano, H. Oike, A. Kikkawa, F. Kagawa, Y. Tokunaga, H. M. Rønnow, Y. Tokura, Y. Taguchi, *Nat. Mater.* **2016**, *15*, 1237.
- [4] S. L. Zhang, F. Kronast, G. van der Laan, T. Hesjedal, *Nano Lett.* **2018**, *18*, 1057.
- [5] S. Seki, X. Z. Yu, S. Ishiwata, Y. Tokura, *Science* **2012**, *336*, 198.
- [6] A. K. Nayak, V. Kumar, T. Ma, P. Werner, E. Pippel, R. Sahoo, F. Damay, U. K. Röbler, S. S. P. Parkin, *Nature* **2017**, *548*, 561.
- [7] P. J. Hsu, A. Kubetzka, A. Finco, N. Romming, K. von Bergmann, R. Wiesendanger, *Nat. Nanotechnol.* **2017**, *12*, 123.
- [8] Y. Cao, A. W. Rushforth, Y. Sheng, H. Z. Zheng, K. Y. Wang, *Adv. Funct. Mater.* **2019**, *29*, 1808104.
- [9] K. M. Cai, M. Y. Yang, H. L. Ju, S. M. Wang, Y. Ji, B. H. Li, K. W. Edmonds, Y. Sheng, B. Zhang, N. Zhang, S. Liu, H. Z. Zheng, K. Y. Wang, *Nat. Mater.* **2017**, *16*, 712.
- [10] W. J. Jiang, G. Chen, K. Liu, J. D. Zang, S. G. E. te Velthuis, A. Hoffmann, *Phys. Rep.* **2017**, *704*, 1.
- [11] F. S. Zheng, H. Li, S. S. Wang, D. S. Song, C. M. Jin, W. S. Wei, A. Kovács, J. D. Zang, M. L. Tian, Y. H. Zhang, H. F. Du, R. E. D. Borkowski, *Phys. Rev. Lett.* **2017**, *119*, 197205.
- [12] G. Q. Yu, P. Upadhyaya, X. Li, W. Y. Li, S. K. Kim, Y. B. Fan, K. L. Wong, Y. Tserkovnyak, P. K. Amiri, K. L. Wang, *Nano Lett.* **2016**, *16*, 1981.
- [13] L. Rózsa, A. Deák, E. Simon, R. Yanes, L. Udvardi, L. Szunyogh, U. Nowak, *Phys. Rev. Lett.* **2016**, *117*, 157205.
- [14] S. Woo, K. Litzius, B. Krüger, M. Y. Im, L. Caretta, K. Richter, M. Mann, A. Krone, R. M. Reeve, M. Weigand, P. Agrawal, I. Lemesch, M. A. Mawass, P. Fischer, M. Kläui, G. S. D. Beach, *Nat. Mater.* **2016**, *15*, 501.
- [15] A. Soumyanarayanan, M. Raju, A. L. G. Oyarce, A. K. C. Tan, M. Y. Im, A. P. Petrovic, P. Ho, K. H. Khoo, M. Tran, C. K. Gan, F. Ernult, C. Panagopoulos, *Nat. Mater.* **2017**, *16*, 898.
- [16] M. He, L. C. Peng, Z. Z. Zhu, G. Li, J. W. Cai, J. Q. Li, H. X. Wei, L. Gu, S. G. Wang, T. Y. Zhao, B. G. Shen, Y. Zhang, *Appl. Phys. Lett.* **2017**, *111*, 202403.

- [17] W. J. Jiang, P. Upadhyaya, W. Zhang, G. Q. Yu, M. B. Jungfleisch, F. Y. Fradin, J. E. Pearson, Y. Tserkovnyak, K. L. Wang, O. Heinonen, S. G. E. te Velthuis, A. Hoffmann, *Science* **2015**, *349*, 283.
- [18] J. Sampaio, V. Cros, S. Rohart, A. Thiaville, A. Fert, *Nanotechnol.* **2013**, *8*, 839.
- [19] S. Meyer, M. Perini, S. von Malottki, A. Kubetzka, R. Wiesendanger, K. von Bergmann, S. Heinze, *Nat. Commun.* **2019**, *10*, 3823.
- [20] M. Raju, A. Yagil, A. Soumyanarayanan, A. K. C. Tan, A. Almoalem, F. S. Ma, O. M. Auslaender, C. Panagopoulos, *Nat. Commun.* **2019**, *10*, 696.
- [21] S. Heinze, K. von Bergmann, M. Menzel, J. Brede, A. Kubetzka, R. Wiesendanger, G. Bihlmayer, S. Blügel, *Nat. Phys.* **2011**, *7*, 713.
- [22] S. D. Pollard, J. A. Garlow, J. W. Yu, Z. Wang, Y. M. Zhu, H. Yang, *Nat. Commun.* **2017**, *8*, 14761.
- [23] J. A. Garlow, S. D. Pollard, M. Beleggia, T. Dutta, H. Yang, Y. M. Zhu, *Phys. Rev. Lett.* **2019**, *122*, 237201.
- [24] D. Liang, J. P. DeGrave, M. J. Stolt, Y. Tokura, S. Jin, *Nat. Commun.* **2015**, *6*, 8217.
- [25] Y. Guang, I. Bykova, Y. Z. Liu, G. Q. Yu, E. Goering, M. Weigand, J. Gräfe, S. K. Kim, J. W. Zhang, H. Zhang, Z. R. Yan, C. H. Wan, J. F. Feng, X. Wang, C. Y. Guo, H. X. Wei, Y. Peng, Y. Tserkovnyak, X. F. Han, G. Schütz, *Nat. Commun.* **2020**, *11*, 949.
- [26] W. J. Jiang, X. C. Zhang, G. Q. Yu, W. Zhang, X. Wang, M. B. Jungfleisch, J. E. Pearson, X. M. Cheng, O. Heinonen, K. L. Wang, *Nat. Phys.* **2017**, *13*, 162.
- [27] L. Caretta, M. Mann, F. Büttner, K. Ueda, B. Pfau, C. M. Günther, P. Helsing, A. Churikova, C. Klose, M. Schneider, D. Engel, C. Marcus, D. Bono, K. Bagschik, S. Eisebitt, G. S. D. Beach, *Nat. Nanotechnol.* **2018**, *13*, 1154.
- [28] Y. Hirata, D. H. Kim, S. K. Kim, D. K. Lee, S. H. Oh, D. Y. Kim, T. Nishimura, T. Okuno, Y. Futakawa, H. Yoshikawa, A. Tsukamoto, Y. Tserkovnyak, Y. Shiota, T. Moriyama, S. B. Choe, K. J. Lee, *Nat. Nanotechnol.* **2019**, *14*, 232.
- [29] T. Jungwirth, X. Marti, P. Wadley, J. Wunderlich, *Nat. Nanotechnol.* **2016**, *11*, 231.
- [30] V. Baltz, A. Manchon, M. Tsoi, T. Moriyama, T. Ono, Y. Tserkovnyak, *Rev. Mod. Phys.* **2018**, *90*, 015005.
- [31] J. Barker, O. A. Tretiakov, *Phys. Rev. Lett.* **2016**, *116*, 147203.
- [32] C. A. Akosa, O. A. Tretiakov, G. Tatara, A. Manchon, *Phys. Rev. Lett.* **2018**, *121*, 097204.
- [33] C. D. Jin, C. K. Song, J. B. Wang, Q. F. Liu, *Appl. Phys. Lett.* **2016**, *109*, 182404.
- [34] L. C. Shen, J. Xia, G. P. Zhao, X. C. Zhang, M. Ezawa, O. A. Tretiakov, X. X. Liu, Y. Zhou, *Phys. Rev. B* **2018**, *98*, 134448.
- [35] B. Göbel, A. Mook, J. Henk, I. Mertig, *Phys. Rev. B* **2017**, *96*, 060406.
- [36] A. F. Pacheco, E. Vedmedenko, F. Ummelen, R. Mansell, D. Petit, R. P. Cowburn, *Nat. Mater.* **2019**, *18*, 679.
- [37] D. S. Han, K. Lee, J. P. Hanke, Y. Mokrousov, K. W. Kim, W. Yoo, Y. L. W. van Hees, T. W. Kim, R. Lavrijsen, C. Y. You, H. J. M. Swagten, M. H. Jung, M. Kläui, *Nat. Mater.* **2019**, *18*, 703.
- [38] W. Legrand, D. Maccariello, F. Ajejas, S. Collin, A. Vecchiola, K. Bouzehouane, N. Reyren, V. Cros, A. Fert, *Nat. Mater.* **2020**, *19*, 34.
- [39] T. Dohi, S. DuttaGupta, S. Fukami, H. Ohno, *Nat. Commun.* **2019**, *10*, 5153.
- [40] S. L. Zhang, Y. Liu, L. J. C. McIntyre, T. Hesjedal, J. Y. Zhang, S. G. Wang, G. H. Yu, *Sci. Rep.* **2013**, *3*, 2087.
- [41] J. Y. Zhang, G. Yang, S. G. Wang, J. L. Liu, R. M. Wang, E. Amsellem, A. Kohn, G. H. Yu, *Appl. Phys. Lett.* **2015**, *106*, 152401.
- [42] X. C. Zhang, Y. Zhou, M. Ezawa, *Nat. Commun.* **2016**, *7*, 10293.
- [43] Y. Y. Dai, H. Wang, P. Tao, T. Yang, W. J. Ren, Z. D. Zhang, *Phys. Rev. B* **2013**, *88*, 054403.
- [44] W. J. Li, I. Bykova, S. L. Zhang, G. Q. Yu, R. Tomasello, M. Carpentieri, Y. Z. Liu, Y. Guang, J. Gräfe, M. Weigand, D. M. Burn, G. van der Laan, T. Hesjedal, Z. R. Yan, J. F. Feng, C. H. Wan, J. W. Wei, X. Wang, X. M. Zhang, H. J. Xu, C. Y. Guo, H. X. Wei, G. Finocchio, X. F. Han, G. Schütz, *Adv. Mater.* **2019**, *31*, 1807683.
- [45] F. S. Zheng, F. N. Rybakov, A. B. Borisov, D. S. Song, S. S. Wang, Z. A. Li, H. F. Du, N. S. Kiselev, J. Caron, A. Kovács, M. L. Tian, Y. H. Zhang, S. Blügel, R. E. D. Borkowski, *Nat. Nanotechnol.* **2018**, *13*, 451.
- [46] Z. Y. Liu, S. Adenwalla, *Phys. Rev. Lett.* **2003**, *91*, 037207.
- [47] I. S. Lobanov, H. Jónsson, V. M. Uzdin, *Phys. Rev. B* **2016**, *94*, 174418.
- [48] D. Stosic, J. Mulkers, B. Van Waeyenberge, T. B. Ludermit, M. V. Milošević, *Phys. Rev. B* **2017**, *95*, 214418.
- [49] J. F. Ankner, G. P. Felcher, *J. Magn. Magn. Mater.* **1999**, *200*, 741.
- [50] T. Zhu, Y. Yang, R. C. Yu, H. Ambaye, V. Lauter, J. Q. Xiao, *Appl. Phys. Lett.* **2012**, *100*, 202406.
- [51] M. Björck, G. Andersson, *J. Appl. Crystallogr.* **2007**, *40*, 1174.
- [52] I. Purnama, W. L. Gan, D. W. Wong, W. S. Lew, *Sci. Rep.* **2015**, *5*, 10620.
- [53] X. C. Zhang, M. Ezawa, Y. Zhou, *Phys. Rev. B* **2016**, *94*, 064406.
- [54] C. Reichhardt, D. Ray, C. J. Olson Reichhardt, *Phys. Rev. Lett.* **2015**, *114*, 217202.
- [55] C. Reichhardt, C. J. Olson Reichhardt, *New J. Phys.* **2016**, *18*, 095005.
- [56] X. Liang, G. P. Zhao, L. C. Shen, J. Xia, L. Zhao, X. C. Zhang, Y. Zhou, *Phys. Rev. B* **2019**, *100*, 144439.